Ultrafast all-optical diffraction switching using semiconductor metasurfaces

Cite as: Appl. Phys. Lett. **118**, 211105 (2021); https://doi.org/10.1063/5.0049585
Submitted: 06 March 2021 . Accepted: 05 May 2021 . Published Online: 26 May 2021

Polina P. Vabishchevich, Aleksandr Vaskin, Nicholas Karl, John L. Reno, Michael B. Sinclair, Isabelle Staude, and Igal Brener

Applied Physics Letters ARTICLE scitation.org/journal/apl

Ultrafast all-optical diffraction switching using semiconductor metasurfaces

Cite as: Appl. Phys. Lett. **118**, 211105 (2021); doi: 10.1063/5.0049585
Submitted: 6 March 2021 · Accepted: 5 May 2021 ·
Published Online: 26 May 2021

Polina P. Vabishchevich,[1,2] Aleksandr Vaskin,[3] Nicholas Karl,[1,2] John L. Reno,[1,2] Michael B. Sinclair,[2] Isabelle Staude,[3,4] and Igal Brener[1,2,a)]

AFFILIATIONS

[1]Sandia National Laboratories, Albuquerque, New Mexico 87185, USA
[2]Center for Integrated Nanotechnologies, Sandia National Laboratories, Albuquerque, New Mexico 87185, USA
[3]Institute of Applied Physics, Abbe Center of Photonics, Friedrich Schiller University Jena, Albert-Einstein-Str. 15, 07745 Jena, Germany
[4]Institute of Solid State Physics, Abbe Center of Photonics, Friedrich Schiller University Jena, Max-Wien-Platz 1, 07743 Jena, Germany

Note: This Paper is part of the APL Special Collection on Metastructures: From Physics to Applications.
[a)]**Author to whom correspondence should be addressed**: ibrener@sandia.gov

ABSTRACT

Ultrafast all-optical switching using Mie resonant metasurfaces requires both on-demand tunability of the wavefront of the light and ultrafast time response. However, devising a switching mechanism that has a high contrast between its "on" and "off" states without compromising speed is challenging. Here, we report the design of a tunable Mie resonant metasurface that achieves this behavior. Our approach utilizes a diffractive array of semiconductor resonators that support both dipolar and quadrupolar Mie resonances. By balancing the strengths of the dipole and quadrupole resonances, we can suppress radiation into the first diffraction order, thus creating a clearly delineated "off"-state at the operating wavelength. Then, we use optical injection of free- carriers to spectrally shift the multipoles and rebalance the multipole strengths, thereby enabling radiation into the diffraction order—all on an ultrafast timescale. We demonstrate ultrafast off-to-on switching with $I_{on}/I_{off} \approx 5$ modulation of the diffracted intensity and ultrafast on-to-off switching with $I_{on}/I_{off} \approx 9$ modulation. Both switches exhibit a fast $\tau_{tr} \approx 2.7$ ps relaxation time at 215 μJ cm^{-2} pump fluence. Further, we show that for higher fluences, the temporal response of the metasurface is governed by thermo-optic effects. This combination of multipole engineering with lattice diffraction opens design pathways for tunable metasurface-based integrated devices.

Optical metasurfaces consist of two-dimensional collections of nanoscale engineered resonators or "meta-atoms," which can provide full control over phase, amplitude, and polarization of light.[1,2] Moreover, using dielectric meta-atoms (such as Mie resonators) exhibiting an optical response dominated by electric and magnetic multipole moments, it is possible to shape the optical wavefront by varying the dimension, shape, and material of each meta-atom and its surroundings. This level of control enables metasurface-based flat-optical components,[3,4] metasurfaces with directional scattering,[5–8] holographic metasurfaces,[9–11] and metasurfaces for nonlinear wavefront shaping.[12] When meta-atoms are arranged in periodic arrays, we can also engineer the diffraction order intensity.[13–18] In this case, the metasurfaces are sometimes called "metagratings" or "metalattices," and their optical response will also be affected by the lattice modes, resonator cross coupling, and the emission patterns of the excited multipoles,[13,19–22] resulting in new functionalities in beam control and manipulation.[13]

While it has long been recognized that metasurfaces have the potential for wavefront shaping, it has been difficult to achieve efficient, high-contrast, all-optical switching while maintaining ultrafast response times. Of the several approaches used to impart a tunable or dynamic behavior to metasurfaces,[23–33] the fastest tunability has been shown using ultrafast laser techniques to manipulate the optical response of semiconductor-based metasurfaces.[34–45] While the studies that employed Kerr and multi-photon absorption nonlinearities achieve extreme ultrafast response,[40–42] ultrafast optical injection of free carriers (FCs) in direct bandgap semiconductors represents an attractive mechanism for achieving the largest absolute modulation depth on a picosecond timescales.[43–45] Injection of free carriers reduces the refractive index of the semiconductor medium, which, in

turn, blue-shifts the Mie resonances. At very high injection levels, free carrier absorption can also dampen and broaden the Mie resonances. The FCs decay within a few picoseconds due to surface recombination, thus providing an ultrafast switching cycle. However, in previous works, the modulation contrast of reflectance was below 40% because the metasurfaces used did not achieve complete suppression of the scattering that defines the baseline signal at the "off"-state. Therefore, to successfully create an all-optical switch that can provide high "on–off" contrast, we must create a metasurface with an "off" state that exhibits minimal scattering.

To address this problem, we utilize a diffractive metasurface whose meta-atoms support both dipolar and quadrupolar Mie resonances at the operating wavelength. Through appropriate design, we can destructively combine the dipolar and quadrupolar radiation into the first diffracted order and thus achieve a high quality "off" state. We utilize quadrupole resonances in our approach because they offer three significant advantages:[46] (i) quadrupoles have fourfold symmetric radiation patterns with lobes at $\pm 45^\circ$ for the $m = 0$ quadrupole; (ii) the radiation lobes of quadrupoles have reduced angular spread compared to those of dipoles; and (iii) the Q-factors of quadrupole resonances tend to be higher than those of dipole resonances, which lowers the required index change to achieve high-contrast all-optical switching. Our approach is similar to the generalized Kerker conditions[7,47] that rely on the spectral and spatial overlap of quadrupole and dipole modes and balanced scattering amplitudes with opposite phases to achieve zero backscattering. However, in our case, we apply the generalized Kerker conditions to a diffracted order.

In this report, we demonstrate this approach using a GaAs-based metasurface. The periodicity of the metasurface is chosen such that a first order diffraction lobe should appear at $\theta_{diff} = -45^\circ$ relative to the metasurface normal for wavelengths near the $m = 0$ magnetic quadrupole (MQ) resonance. By appropriately engineering the relative weights and phases of all the multipoles excited by an incident wave, we are able to suppress the first order diffraction, forming a "latent" diffraction order (Fig. 1). We then use ultrafast optical injection of FCs to shift the wavelength of maximum suppression, thereby enabling diffraction at the operating wavelength. At the wavelength of suppressed diffraction for the unpumped metasurface, we demonstrate an

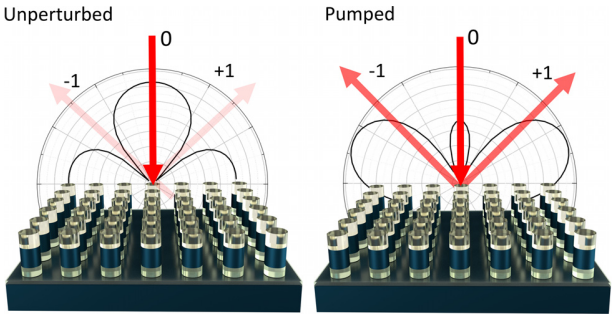

FIG. 1. Illustration of the overlap of the radiation lobes of the magnetic quadrupole mode of a single resonator with the diffraction orders of the metasurface. Left: when the magnetic quadrupole resonance spectrally and spatially overlaps with one of the diffraction orders, full suppression of the -1 diffraction order can be achieved. Right: radiation into the diffraction order can be restored via optical pumping.

ultrafast "turn on" of the diffracted order, followed by relaxation to the "off" state within a few picoseconds, resulting in an ultrafast switching cycle time. We also observe an ultrafast "turn off" of the diffracted order at the shifted wavelength of suppression, followed by a fast relaxation to the "on" state.

The metasurface was fabricated using standard electron-beam lithography and inductively coupled plasma (ICP) etching; details of the fabrication process are described in our previous work.[35] The metasurface consists of a two-dimensional array of three-layer pillars, with the GaAs nanodisk resonator sandwiched between two low refractive index oxide layers. The GaAs nanodisk has a height of 300 nm and a radius of ~200 nm, and supports Mie resonances in the near-IR spectral range. Because we want to manipulate the intensity of a diffracted order near the Mie quadrupole resonances (~1000 nm), the period in the y-direction is chosen to be $p_y = 1200$ nm which allows for diffracted modes at this wavelength. Furthermore, by choosing an incidence angle of $\theta_{inc} = 8^\circ$, we can tune the -1 diffracted order (at ~1000 nm) to $\theta_{diff} = -45^\circ$ in the y-z plane with respect to the array normal [see Fig. 2(a) for definition of axes]. The array period in the x-direction is chosen to be $p_x = 900$ nm so that the array is non-diffractive (in free space) in this direction. Scanning electron micrographs of the fabricated GaAs metasurface are shown in Figs. 2(a) and 2(b).

Measured and numerically simulated spectra of the GaAs metasurface (obtained under normal incidence with the polarization of light along x-direction) are shown in Fig. 2(c). The simulations were performed using the commercial software package COMSOL Multiphysics. The two most prominent features correspond to the magnetic dipole (MD) resonance at ~1350 nm and the magnetic quadrupole resonance (MQ) at ~980 nm. Numerically simulated spectra for the 0 and -1 diffraction orders for $\theta_{inc} = 8^\circ$ are shown in Fig. 2(d). Note that for the simulation of the diffracted order, the angle of diffraction varies with wavelength, and the diffracted order is at -45° for a wavelength of 1015 nm [the upper axis Fig. 2(d) shows the diffraction angle of the -1 order over this wavelength range]. The simulated spectrum of the -1 diffraction order has two minima that correspond to quadrupole-assisted suppression of radiation, one at 1005 nm and another at 1035 nm. To identify the specific Mie-modes responsible for the observed suppression of radiation, we use the method described in Grahn *et al.*[48] to perform a multipolar decomposition [Fig. 2(e)]. We see that the $m = 0$ magnetic quadrupole resonance (MQ_0) is the dominant quadrupole mode at 1035 nm, and its strength is comparable to the electric and magnetic dipole modes [shown with dashed lines, Fig. 2(e)]. Thus, we believe that it is the superposition of the MQ_0 scattering with the dipolar scattering that leads to the suppression at 1035 nm. At the 1005 nm suppression wavelength, a combination of the $m = 1$ and $m = 2$ quadrupole resonances dominates and contributes to the suppression. Since near-complete suppression of diffraction is achieved near 1035 nm, we will concentrate on the suppression near this wavelength for our all-optical switching experiments.

Our experiment [see Fig. 3(a)] is based on a pump-probe transient diffraction spectroscopy setup, with an 800 nm pump pulse, $\tau_{pulse} \sim 85$ fs duration, and ~140 μm beam size. The pump central wavelength, 800 nm, was chosen to be in the absorption band of the GaAs that has a bandgap at 870 nm. A probe pulse is a supercontinuum with a spectral coverage from 920 to 1400 nm. The probe beam,

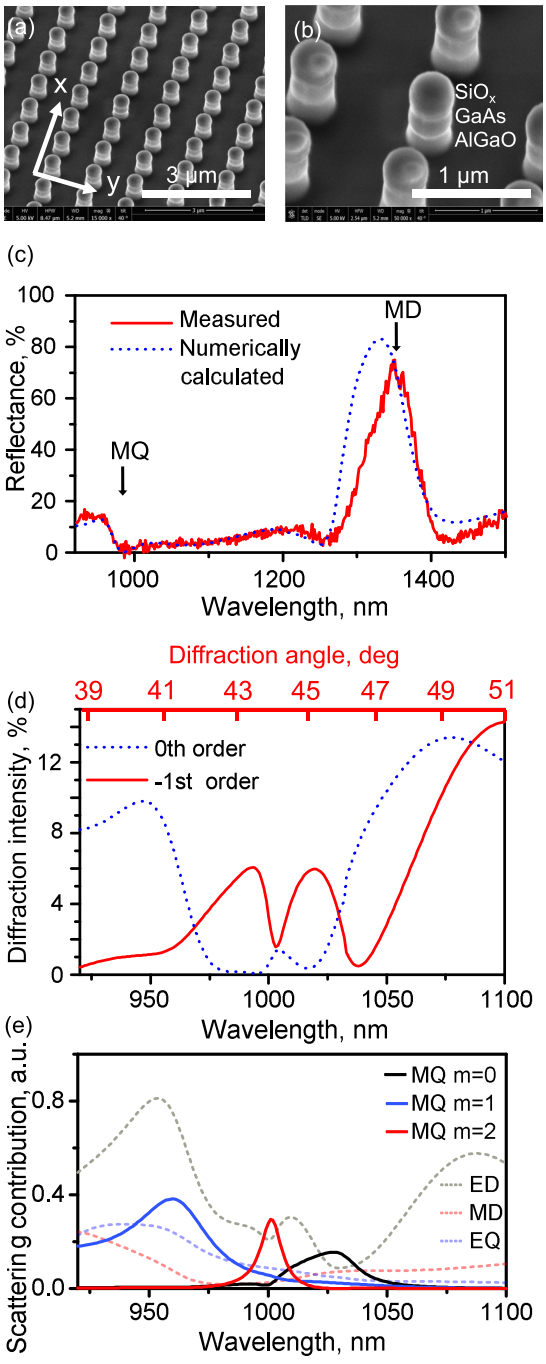

FIG. 2. (a) and (b) A 40° side view scanning electron microscope images of the fabricated GaAs metasurface. (c) Measured (solid red line) and numerically calculated (dashed blue line) reflectance spectra of the GaAs metasurface under normal incidence. Arrows indicate the magnetic dipole (MD) and magnetic quadrupole resonances (MQ). (d) Simulated spectra of the zeroth diffraction order (dashed blue line) and of the −1 diffraction order (red solid line). The upper axis shows the diffraction angle of the −1 diffraction order corresponding to each wavelength. (e) Multipole decomposition of the scattered fields in the metasurface for 8° of incidence. Solid lines correspond to the contributions from MQ modes.

polarized along p_x period, was focused onto the sample with a 150 mm focal length lens and contained an angular spread of ±0.4°. For the experiment, the probe incidence angle was fine tuned to 9° ± 1° to achieve the deepest spectral minimum in the diffracted spectrum. We employ two collection channels: one for the reflected zero-order beam and another for the −1 diffraction order centered at $\theta_{diff} = -45°$ with respect to the sample normal. The diffraction channel collects scattering with an angular spread of ±3.5° (see the supplementary material Fig. S1).

The experimentally measured spectrum of the −1 diffraction order at $\theta_{diff} = -45°$ as a function of pump power is shown in Fig. 3(b). These measurements were obtained with a pump-probe delay of 0 ps, which corresponds to the maximum pump-induced changes of the diffraction spectra. Note that the finite spectral width of these spectra is due to the ±3.5° range of collection angles. For zero pump fluence, we observe a minimum in the diffraction spectrum at 1048 nm. We associate this minimum with suppression due to the MQ_0 mode which is observed at 1034 nm in the numerical simulations. We believe that this discrepancy is mostly due to the change of incidence angle from 8° to 9° ± 1°, but also to slight deviations between the designed structure and the fabricated structure. We see that as the pump fluence is increased from 0 to 600 $\mu J\ cm^{-2}$, the spectral position of the diffraction minimum blue-shifts up to $\Delta\lambda = -25$ nm due to the decrease in refractive index caused by band filling (BF), band shrinkage (BS), and Drude contributions.[43,44] From the data of Fig. 3(b), we observe that at a pump fluence of 215 $\mu J\ cm^{-2}$ (which corresponds to an estimated FC density of $N_0 \sim 3 \times 10^{19}\ cm^{-3}$), the diffraction minimum rigidly shifts by about its full width, leading to the appearance of substantial intensity in the initially suppressed diffracted order at 1048 nm. This is the "on" state for this wavelength.

The data of Fig. 3(b) also show high contrast on-to-off switching at 1034 nm which is the wavelength of the shifted minimum. In fact, the switching contrast (defined below) is better at 1034 nm. Figure 3(c) shows the intensity at zero delay for 1048 and 1034 nm as a function of pump fluence. The measured intensity is normalized to the maximum observed intensity over this fluence range. For the off-to-on switching at 1048 nm, I/I_{max} continues to increase with pump fluence, while for on-to-off switching at 1034 nm a minimum, I/I_{max} is observed near 215 $\mu J\ cm^{-2}$. Working with pump fluences of 0 and 215 $\mu J\ cm^{-2}$, and associating the maximum and minimum I/I_{max} at each of the switching wavelengths with the "on" and "off" states, we obtain switching contrasts of $I_{on}/I_{off} \approx 5$ for 1048 nm and $I_{on}/I_{off} \approx 9$ at 1034 nm. Figure 3(d) shows the (unnormalized) diffracted spectra for the unpumped state ($F = 0\ \mu J\ cm^{-2}$) and the pumped state ($F = 215\ \mu J\ cm^{-2}$). The dashed lines in Fig. 3(d) mark the locations of the two switching regimes.

To demonstrate that our GaAs metasurface has an ultrafast response, we optically pump with a fluence of $F = 215\ \mu J\ cm^{-2}$ and measure transient diffraction spectra in the delay range from −3 to 20 ps. Figure 4(a) shows measured unnormalized spectra. It is clearly seen that the spectral minimum observed near 1048 nm for negative time delays shifts toward shorter wavelengths with time as the resonance frequencies of the dipole and quadrupole modes increases. Figure 4(b) shows the switching transient recorded for 1048 nm. An instrument-limited ultrafast "turn on" of the diffracted mode is observed followed by picosecond timescale relaxation back to the "off"-stated. Figure 4(c) shows the corresponding data for 1034 nm

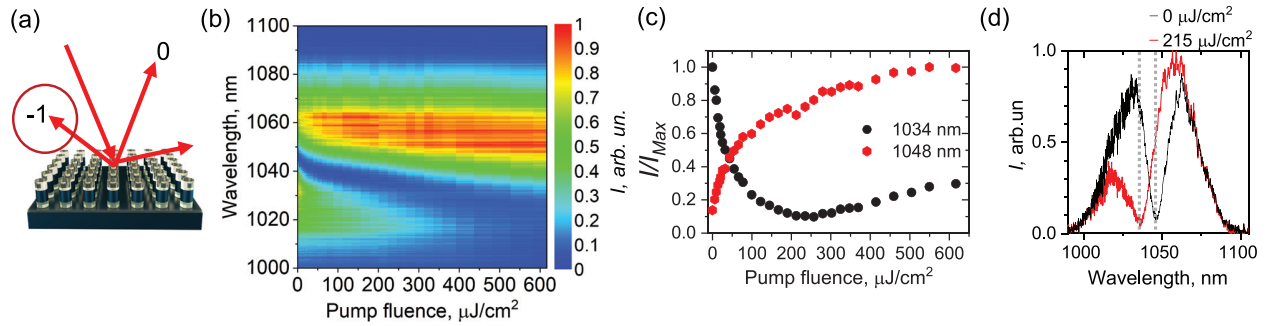

FIG. 3. (a) A schematic of the experiment. (b) Measured unnormalized diffraction spectra as a function of the pump fluence. The spectra were recorded at zero time delay which corresponds to the maximum pump induced changes. (c) The measured diffraction intensity at zero time delay for 1048 and 1034 nm as a function of pump fluence. The intensity curves are normalized to the maximum intensity at each wavelength. (d) Measured spectrum of the −1 diffraction order in the absence (black curve) and presence (red curve) of optical pumping. The dashed curves show the switching wavelengths of 1048 and 1034 nm.

where an instrument-limited switching from "on" to "off" is followed by picosecond timescale relaxation to the "on" state. In both cases, the temporal dynamics at positive time-delays are controlled by single-photon absorption (SPA) and two-photon absorption (TPA) processes, followed by FC exponential decay with $\tau_{tr} = 2.7$ ps relaxation time. At $\tau = 10$ ps, the diffracted intensity recovers completely to the unpumped state, demonstrating ultrafast all-optical switching (changes after 10 ps are almost negligible). Thus, these experimental results prove that quadrupole-assisted scattering suppression can provide the required zero baseline for high-modulation contrast at an ultrafast speed, which makes this approach promising for future of ultrafast all-optical switching applications.

At higher pumping fluences, we discovered a secondary challenge: pump-induced thermo-optic effects can significantly prolong metasurface response time and negatively impact the duty cycle of the all-optical switch. To explore this process, we measure a set of the transient spectra of the GaAs metasurface when it is pumped with higher-than-optimal fluences (see the supplementary material Figs. S2 and S3). Figure 5(a) shows the time-dependent differential diffraction spectra, $\Delta I/I_0$, using a pump fluence of $F = 550$ μJ cm^{-2} (note that the differential diffraction spectra are different from the raw spectra shown in Fig. 4). For time delays τ between 0 and 10 ps, the evolution of the spectrum is dominated by the time dependent density of optically generated FCs [$\tau = 0.1$ ps is shown in Fig. 5(b) in blue]. In contrast, for $\tau > 10$ ps, the metasurface response is governed by thermo-optic effects: carrier-phonon interactions that heat the GaAs resonators. At $\tau = 20$ ps [Fig. 5(b), red curve], the spectral position of the diffraction dip is red shifted by $\Delta\lambda \sim 1.5$ nm compared to the unperturbed diffraction spectrum [Fig. 5(b), black curve]. In most semiconductors, the bandgap decreases with increasing temperature, which increases the refractive index and causes a red-shift of the Mie resonances. In addition to the red-shift observed at $\tau = 20$ ps, there is an overall decrease in the diffraction suppression (and thus the switching contrast), caused by increased absorption in the GaAs metasurface as the temperature is increased. Therefore, the thermal modification of the refractive index at longer timescales significantly extends the relaxation time in optically pumped metasurfaces and deteriorates the performance of the all-optical switch. These thermo-optic effects thus limit the amount of fluence that can be used to tune the resonance while preserving picosecond relaxation time and high contrast switching modulation.

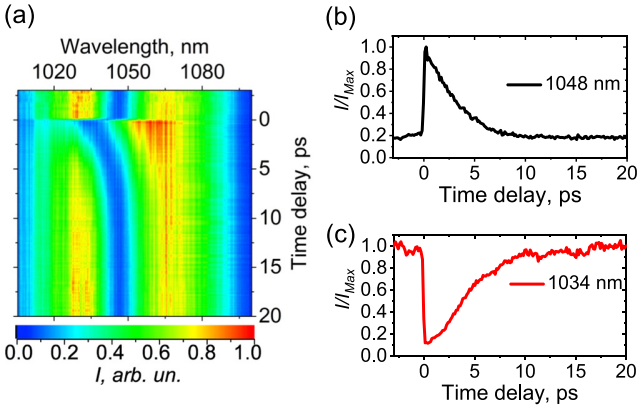

FIG. 4. The pump-probe measurements of −1 diffraction order in the spectral vicinity of the $m = 0$ magnetic quadrupole resonance. (a) Measured unnormalized spectra of the −1 diffraction order as a function of the probe wavelength and the time delay between pump and probe pulses. Pump fluence is $F = 215$ μJ cm^{-2}. (b) Intensity at 1048 nm as a function of time showing fast off-to-on switching followed by fast decay to the "off" state. (c) Intensity at 1034 nm as a function of time showing fast on-to-off switching followed by fast recovery of the "on" state. The time traces in (b) and (c) are normalized by their maximum intensity.

To validate our explanation for the observed experimental behavior, we provide a numerical model of our results. We use simple rate equations to describe the carrier-induced time-dependent characteristics of our system,[40,43,44,49]

$$\dot{N(t)} = -\left(AN(t) + BN(t)^2 + C_{eff}N(t)^3\right),$$
$$C_{GaAs}\dot{T}(t) = E_{BG}\left(AN(t) + C_{eff}N(t)^3\right).$$

The first equation describes the FC density dynamics $N(t)$. As shown in our previous works,[43,44] A is the monomolecular coefficient mediating nonradiative decay from defects and surface states that defines the fast surface recombination rate $A = 1/\tau_{tr}$ ($A = 3.7 \times 10^{11}$ s^{-1}). B is the bimolecular coefficient for recombination with radiation emission and C_{eff} is the effective Auger coefficient. B and C_{eff} parameters are

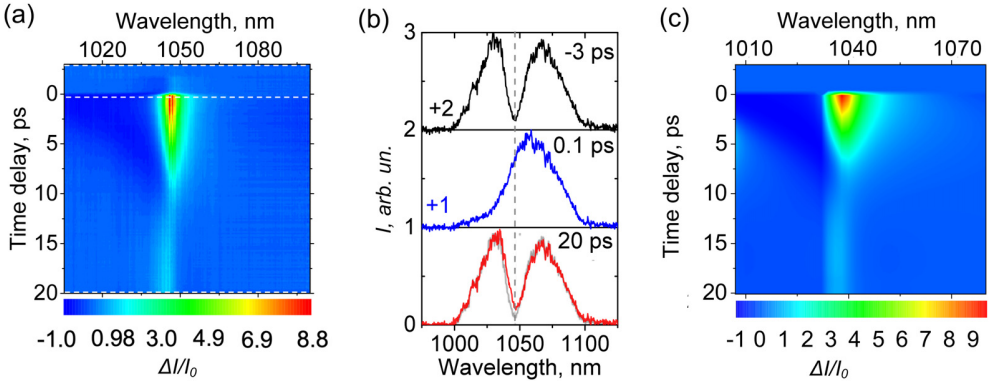

FIG. 5. Pump-probe measurements of −1 diffraction order in the spectral vicinity of the $m = 0$ magnetic quadrupole resonance, for pump fluence of $F = 550\ \mu J\ cm^{-2}$. (a) Transient differential intensity of the −1 diffraction order spectra. Dashed lines correspond to the measured spectra shown in (b). (b) Measured spectra of −1 diffraction order for three different time-delays ($\tau = -3$ ps, $\tau = 0.1$ ps, $\tau = 20$ ps) between pump and probe pulses. The spectrum for $\tau = -3$ ps (black curve) is the same as for the unpumped sample. The spectrum for $\tau = 0.1$ ps (blue curve) reveals significant blue-shift of the dip and suppression of diffraction in the 1050–1030 nm spectral window. The spectrum for $\tau = 20$ ps (red curve) reveals slight red-shift and loss of suppression (gray curve shows spectrum for −3 ps that corresponds to the unperturbed spectrum of the unpumped metasurface). (c) Numerically simulated differential intensity, including thermo-optic effects.

assumed to be the same as for bulk GaAs ($B = 1.7 \times 10^{-10}\ cm^3\ s^{-1}$, $C_{eff} = 7 \times 10^{-30}\ cm^6\ s^{-1}$); however, they play a negligible role in comparison with surface recombination. The initial density of injected FCs was estimated as $N_0 = 2F(1-e^{-kxd})/dE_{pump}$, where $d = 300$ nm is the metasurface thickness, $\alpha = 1.44 \times 10^4\ cm^{-1}$ is the GaAs linear absorption coefficient at 800 nm, $E_{pump} = 1.55$ eV, and F is the pump fluence. To take into account the difference in the spectral shift of the resonance obtained in the experiment with the spectral shift achieved with this model, we introduce a coefficient $k = 2$ that provides an increase in absorption and increase number of generated free carriers. The second equation describes the simplified dependence of the GaAs metasurface temperature $T(t)$ on the nonradiative recombination processes that contribute to the heating. Here, the bandgap energy of GaAs is E_{BG}, and the volume-specific heat of GaAs is $C_{GaAs} = 1.74\ J\ K^{-1}\ cm^{-3}$.[50] This equation describes the rise in temperature of GaAs nanodisks and does not provide an explicit model for non-homogeneous heat dissipation in the nanostructure. Using this model, we simulated the metasurface response including both free carrier and thermo-optic effects. While a relatively good agreement was found for the spectral shift of the resonance, the changes in the spectral width of the resonance were found to be significantly larger in the experiment; thus, they were estimated from the experimental data (see the supplementary material for full details). The results, shown in Fig. 5(c) for the fluence of $F = 550\ \mu J\ cm^{-2}$ that corresponds to an initial plasma density of $N_0 = 8 \times 10^{-19}\ cm^{-3}$, compare favorably with the measured spectra, and confirm that thermo-optic effects are indeed impacting the longer time spectra.

In conclusion, our results show diffraction switching, utilizing the quadrupole-assisted suppression to clearly delineate the switch's "off" state which results in a high contrast ($I_{on}/I_{off} \approx 5$) off-to-on switching. We also observed a second switching regime in which on-to-off switching occurs with a contrast ratio of $I_{on}/I_{off} \approx 9$. In both cases, we observe a fast relaxation to the unswitched state with a $\tau_{tr} \approx 2.7$ ps relaxation time. The absolute intensity of the diffraction order in our GaAs metasurface is less than 10%; however, a similar strategy can be used to design GaAs metasurface with suppression of the zero order diffraction, which will significantly improve the absolute modulation values and surpass the present results. Additionally, we show that at high fluences, the long-time temporal response of the metasurface is dominated by thermo-optic effects, and, in our case, only pump fluences up to about 215 $\mu J\ cm^{-2}$ can be used to preserve ultrafast switching times. This limiting pump fluence impacts the metasurface design and dictates the minimum Q-factor of the resonance that can be used for ultrafast all-optical switching. Our work demonstrates the great potential of high-order Mie-modes in metasurfaces for wavefront shaping and provides a critical step toward creating metasurface-based integrated devices that are tunable at ultrafast speeds.

See the supplementary material for experimental setup details (Fig. S1) and transient intensity of the −1 diffraction order spectra for different pump fluences (Figs. S2 and S3).

The authors thank Maxim Shcherbakov for the initial discussion of the experiment. This work was supported by the U.S. Department of Energy, Office of Basic Energy Sciences, Division of Materials Sciences and Engineering and performed, in part, at the Center for Integrated Nanotechnologies, an Office of Science User Facility operated for the U.S. Department of Energy (DOE) Office of Science. Sandia National Laboratories is a multi-mission laboratory managed and operated by National Technology and Engineering Solutions of Sandia, LLC, a wholly owned subsidiary of Honeywell International, Inc., for the U.S. Department of Energy's National Nuclear Security Administration under Contract No. DE-NA0003525. This paper describes objective technical results and analysis. Any subjective views or opinions that might be expressed in the paper do not necessarily represent the views of the U.S. Department of Energy or the United States Government. A.V. and I.S. acknowledge the financial support from the German Research Foundation (No. STA 1426/2-1).

A.V., P.P.V., and J.L.R., fabricated metasurface samples. P.P.V. and A.V. performed experimental measurements. A.V., P.P.V., and

N.K. performed numerical simulations. All authors contributed to the metasurface design development, the analysis of the results, and the manuscript editing. P.P.V. and A.V. contributed equally to this work.

DATA AVAILABILITY

The data that support the findings of this study are available from the corresponding author upon reasonable request.

REFERENCES

[1]A. Arbabi, Y. Horie, M. Bagheri, and A. Faraon, Nat. Nanotechnol. **10**, 937 (2015).
[2]Y. F. Yu, A. Y. Zhu, R. Paniagua-Domínguez, Y. H. Fu, B. Luk'yanchuk, and A. I. Kuznetsov, Laser Photonics Rev. **9**, 412 (2015).
[3]N. Yu and F. Capasso, Nat. Mater. **13**, 139 (2014).
[4]J. B. Mueller, K. Leosson, and F. Capasso, Optica **3**, 42 (2016).
[5]I. Staude, A. E. Miroshnichenko, M. Decker, N. T. Fofang, S. Liu, E. Gonzales, J. Dominguez, T. S. Luk, D. N. Neshev, and I. Brener, ACS Nano **7**, 7824 (2013).
[6]S. Campione, L. I. Basilio, L. K. Warne, and M. B. Sinclair, Opt. Express **23**, 2293 (2015).
[7]A. Pors, S. K. H. Andersen, and S. I. Bozhevolnyi, Opt. Express **23**, 28808 (2015).
[8]H. K. Shamkhi, K. V. Baryshnikova, A. Sayanskiy, P. Kapitanova, P. D. Terekhov, P. Belov, A. Karabchevsky, A. B. Evlyukhin, Y. Kivshar, and A. S. Shalin, Phys. Rev. Lett. **122**, 193905 (2019).
[9]X. Ni, A. V. Kildishev, and V. M. Shalaev, Nat. Commun. **4**, 2807 (2013).
[10]G. Zheng, H. Mühlenbernd, M. Kenney, G. Li, T. Zentgraf, and S. Zhang, Nat. Nanotechnol. **10**, 308 (2015).
[11]B. Wang, F. Dong, Q.-T. Li, D. Yang, C. Sun, J. Chen, Z. Song, L. Xu, W. Chu, and Y.-F. Xiao, Nano Lett. **16**, 5235 (2016).
[12]L. Wang, S. Kruk, K. Koshelev, I. Kravchenko, B. Luther-Davies, and Y. Kivshar, Nano Lett. **18**, 3978 (2018).
[13]W. Liu and A. E. Miroshnichenko, ACS Photonics **5**, 1733 (2017).
[14]Z. Fan, M. R. Shcherbakov, M. Allen, J. Allen, B. Wenner, and G. Shvets, ACS Photonics **5**, 4303 (2018).
[15]Z. Zhang, M. Kang, X. Zhang, X. Feng, Y. Xu, X. Chen, H. Zhang, Q. Xu, Z. Tian, and W. Zhang, Adv. Mater. **32**(36), 2002341 (2020).
[16]Y. Ra'di, D. L. Sounas, and A. Alù, Phys. Rev. Lett. **119**, 067404 (2017).
[17]Y. Liu, H. Zhou, and J. Zhang, Sci. Rep. **10**, 1 (2020).
[18]T. Shi, Y. Wang, Z. L. Deng, X. Ye, Z. Dai, Y. Cao, B. O. Guan, S. Xiao, and X. Li, Adv. Opt. Mater. **7**(24), 1901389 (2019).
[19]V. E. Babicheva and A. B. Evlyukhin, Laser Photonics Rev. **11**, 1700132 (2017).
[20]V. Babicheva, I. Staude, and D. Gérard, JOSA B **36**, CEC1 (2019).
[21]V. E. Babicheva and A. B. Evlyukhin, Phys. Rev. B **99**, 195444 (2019).
[22]A. D. Utyushev, V. I. Zakomirnyi, and I. L. Rasskazov, Rev. Phys. **6**, 100051 (2021).
[23]A. Komar, R. Paniagua-Dominguez, A. Miroshnichenko, Y. F. Yu, Y. S. Kivshar, A. I. Kuznetsov, and D. Neshev, ACS Photonics **5**, 1742 (2018).
[24]A. Komar, Z. Fang, J. Bohn, J. Sautter, M. Decker, A. Miroshnichenko, T. Pertsch, I. Brener, Y. S. Kivshar, and I. Staude, Appl. Phys. Lett. **110**, 071109 (2017).
[25]M. Decker, C. Kremers, A. Minovich, I. Staude, A. E. Miroshnichenko, D. Chigrin, D. N. Neshev, C. Jagadish, and Y. S. Kivshar, Opt. Express **21**, 8879 (2013).
[26]S. M. Kamali, E. Arbabi, A. Arbabi, Y. Horie, and A. Faraon, Laser Photonics Rev. **10**, 1002 (2016).
[27]P. C. Wu, R. A. Pala, G. Kafaie Shirmanesh, W.-H. Cheng, R. Sokhoyan, M. Grajower, M. Z. Alam, D. Lee, and H. A. Atwater, Nat. Commun. **10**, 1 (2019).
[28]A. Howes, W. Wang, I. Kravchenko, and J. Valentine, Optica **5**(7), 787–792 (2018).
[29]C. Choi, S. Lee, S. Mun, G. Lee, J. Sung, H. Yun, J. Yang, H. Kim, C. Hwang, and B. Lee, Adv. Opt. Mater. **7**, 1900171 (2019).
[30]J. Li, P. Yu, S. Zhang, and N. Liu, Nat. Commun. **11**, 3574 (2020).
[31]S.-Q. Li, X. Xu, R. M. Veetil, V. Valuckas, R. Paniagua-Domínguez, and A. I. Kuznetsov, Science **364**, 1087 (2019).
[32]A. M. Shaltout, V. M. Shalaev, and M. L. Brongersma, Science **364**, eaat3100 (2019).
[33]L. Kang, R. P. Jenkins, and D. H. Werner, Adv. Opt. Mater. **7**, 1801813 (2019).
[34]D. G. Baranov, S. V. Makarov, V. A. Milichko, S. I. Kudryashov, A. E. Krasnok, and P. A. Belov, ACS Photonics **3**, 1546 (2016).
[35]T. Shibanuma, T. Matsui, T. Roschuk, J. Wojcik, P. Mascher, P. Albella, and S. A. Maier, ACS Photonics **4**, 489 (2017).
[36]M. R. Shcherbakov, R. Lemasters, Z. Fan, J. Song, T. Lian, H. Harutyunyan, and G. Shvets, Optica **6**, 1441 (2019).
[37]S. Liu, P. P. Vabishchevich, A. Vaskin, J. L. Reno, G. A. Keeler, M. B. Sinclair, I. Staude, and I. Brener, Nat. Commun. **9**, 2507 (2018).
[38]M. R. Shcherbakov, P. P. Vabishchevich, I. Brener, and G. Shvets, in *Nonlinear Meta-Optics*, edited by C. De Angelis, G. Leo, and D. N. Neshev (CRC Press, 2020), pp. 181–197.
[39]G. Grinblat, H. Zhang, M. P. Nielsen, L. Krivitsky, R. Berté, Y. Li, B. Tilmann, E. Cortés, R. F. Oulton, and A. I. Kuznetsov, Sci. Adv. **6**, eabb3123 (2020).
[40]M. R. Shcherbakov, P. P. Vabishchevich, A. S. Shorokhov, K. E. Chong, D.-Y. Choi, I. Staude, A. E. Miroshnichenko, D. N. Neshev, A. A. Fedyanin, and Y. S. Kivshar, Nano Lett. **15**, 6985 (2015).
[41]G. D. Valle, B. Hopkins, L. Ganzer, T. Stoll, M. Rahmani, S. Longhi, Y. S. Kivshar, C. D. Angelis, D. N. Neshev, and G. Cerullo, ACS Photonics **4**, 2129 (2017).
[42]Y. Yang, W. Wang, A. Boulesbaa, I. I. Kravchenko, D. P. Briggs, A. Puretzky, D. Geohegan, and J. Valentine, Nano Lett. **15**, 7388 (2015).
[43]M. R. Shcherbakov, S. Liu, V. V. Zubyuk, A. Vaskin, P. P. Vabishchevich, G. Keeler, T. Pertsch, T. V. Dolgova, I. Staude, and I. Brener, Nat. Commun. **8**, 1 (2017).
[44]N. Karl, P. P. Vabishchevich, S. Liu, M. B. Sinclair, G. A. Keeler, G. M. Peake, and I. Brener, Appl. Phys. Lett. **115**, 141103 (2019).
[45]N. Karl, P. P. Vabishchevich, M. R. Shcherbakov, S. Liu, M. B. Sinclair, G. Shvets, and I. Brener, Nano Lett. **20**, 7052 (2020).
[46]A. Vaskin, S. Liu, S. Addamane, P. P. Vabishchevich, Y. Yang, G. Balarishnan, M. B. Sinclair, T. Pertsch, I. Brener, and I. Staude, Opt. Express **29**, 5567 (2021).
[47]R. Alaee, R. Filter, D. Lehr, F. Lederer, and C. Rockstuhl, Opt. Lett. **40**, 2645 (2015).
[48]P. Grahn, A. Shevchenko, and M. Kaivola, New J. Phys. **14**, 093033 (2012).
[49]A. de Rossi, M. Lauritano, S. Combrié, Q. V. Tran, and C. Husko, Phys. Rev. A **79**, 043818 (2009).
[50]J. S. Blakemore, J. Appl. Phys. **53**, R123 (1982).